Journal of Controlled Release 209 (2015) 170–178

Contents lists available at ScienceDirect

Journal of Controlled Release

journal homepage: www.elsevier.com/locate/jconrel

# A cleavable cytolysin–neuropeptide Y bioconjugate enables specific drug delivery and demonstrates intracellular mode of action

Verena M. Ahrens [a,1], Katja B. Kostelnik [a,1], Robert Rennert [b], David Böhme [a], Stefan Kalkhof [c], David Kosel [b], Lutz Weber [b], Martin von Bergen [c,d,e], Annette G. Beck-Sickinger [a,*]

[a] Faculty of Biosciences, Pharmacy and Psychology, Institute of Biochemistry, Universität Leipzig, Brüderstraße 34, 04103 Leipzig, Germany
[b] OntoChem GmbH, Heinrich-Damerow-Straße 4, 06120 Halle (Saale), Germany
[c] Department of Proteomics, Helmholtz Centre for Environmental Research - UFZ, Permoserstraße 15, 04318 Leipzig, Germany
[d] Department of Metabolomics, Helmholtz Centre for Environmental Research - UFZ, Permoserstraße 15, 04318 Leipzig, Germany
[e] Department of Biotechnology, Chemistry and Environmental Engineering, University of Aalborg, Denmark

ARTICLE INFO

*Article history:*
Received 14 February 2015
Received in revised form 26 April 2015
Accepted 27 April 2015
Available online 30 April 2015

*Keywords:*
Peptide–drug conjugate
Neuropeptide Y
Cytolysin
Breast cancer
SILAC
Quantitative proteomics

ABSTRACT

Myxobacterial tubulysins are promising chemotherapeutics inhibiting microtubule polymerization, however, high unspecific toxicity so far prevents their application in therapy. For selective cancer cell targeting, here the coupling of a synthetic cytolysin to the $hY_1$-receptor preferring peptide [$F^7$,$P^{34}$]-neuropeptide Y (NPY) using a labile disulfide linker is described. Since $hY_1$-receptors are overexpressed in breast tumors and internalize rapidly, this system has high potential as peptide–drug shuttle system. Molecular characterization of the cytolysin–[$F^7$,$P^{34}$]-NPY bioconjugate revealed potent receptor activation and receptor-selective internalization, while viability studies verified toxicity. Triple SILAC studies comparing free cytolysin with the bioconjugate demonstrated an intracellular mechanism of action regardless of the delivery pathway. Treatments resulted in a regulation of proteins implemented in cell cycle arrest confirming the tubulysin-like effect of the cytolysin. Thus, the cytolysin–peptide bioconjugate fused by a cleavable linker enables a receptor-specific delivery as well as a potent intracellular drug-release with high cytotoxic activity.



## 1. Introduction

Over the past decades numerous anticancer drugs have been developed, but pharmacological research is still challenged by the major issue of selectivity. Therefore, the treatment of tumor diseases currently undergoes a paradigm shift, increasingly directing drug development towards so-called targeted therapeutics. The basic prerequisite of such novel drugs is the distinction between tumor and non-transformed cells in order to reduce and avoid serious side-effects, which up to now are the substantial drawbacks of conventional tumor therapeutics. To meet this issue, targeted therapeutics recognize and address tumor-specific marker molecules, e.g. tumor-associated membrane proteins, or tumor-specific metabolic or regulatory characteristics.

Within the past years, peptide–drug conjugates (PDCs) have been suggested as promising compounds in targeted therapy approaches due to their small size and high selectivity [1]. Herein, a toxic substance is coupled to a peptide, which selectively transports its cargo to the desired site of action [2,3]. However, it is still not clear whether these PDCs address the same intracellular targets as the free drugs since modification and transportation route may alter their characteristics. To address this issue, advances in mass spectrometric methodology revealed SILAC (stable isotope labeling by amino acids in cell culture) as the method of choice to analyze changes in the protein abundance pattern upon treatment in cellular model systems [4]. SILAC depends on the complete metabolic labeling of the cellular proteome and the use of a variation of isotope-labeled amino acids results in differently labeled cell populations [5]. Experimental conditions can then be implemented on the one state, while the other set of cells is kept as a control. If unlabeled and labeled samples are mixed together and analyzed by mass spectrometry, the proteins or peptides will differ in a residue-specific mass shift. Thus, the corresponding signal intensities allow a quantitative comparison of protein abundance in the differently treated cell populations [6].

Here, a novel, site-specifically cleavable PDC for the treatment of breast cancer is described, which is the most frequent tumor disease in the western world's females [7]. Breast cancer cells and metastases are known to express the human $Y_1$-receptor ($hY_1R$) in high density [8] and rapid internalization of this receptor and its corresponding peptide render possible its use as a peptide–drug shuttle system [9]. The $hY_1R$ belongs to the Y-receptor family, consisting of four G protein coupled receptors ($hY_1R$, $hY_2R$, $hY_4R$ and $hY_5R$), which in turn are activated by their natural ligands neuropeptide Y (NPY), peptide YY (PYY),

* Corresponding author.
*E-mail address:* beck-sickinger@uni-leipzig.de (A.G. Beck-Sickinger).
[1] V. M. Ahrens and K. B. Kostelnik contributed equally to this work.

http://dx.doi.org/10.1016/j.jconrel.2015.04.037
0168-3659/

and pancreatic polypeptide (PP) in a multi-ligand/multi-receptor system [10]. Previous research demonstrated that during neoplastic transformation of breast tissue a switch from $hY_2R$- to $hY_1R$-expression occurs, suggesting the $hY_1R$ as a possible breast tumor marker [8]. Hereon after, the sequence-modified NPY analog [$F^7$,$P^{34}$]-NPY, which exhibited high $hY_1R$ preference compared to $hY_2R$ [11], was selectively labeled with $^{99m}$Tc and confirmed the in vivo suitability as breast tumor marker [12].

To advance this concept and transfer its therapeutic application, we here describe for the first time a modified analog of [$F^7$,$P^{34}$]-NPY coupled to a potent, microtubule-disrupting toxin, derived from the myxobacterial tubulysins [13]. The use of a cleavable disulfide linker was designed to release the toxic cargo following peptide-receptor internalization. In order to demonstrate receptor selectivity and cytotoxic efficiency, in vitro testing was performed and finally, the molecular effects induced by the bioconjugate were analyzed by quantitative proteomic analysis in two different breast cancer cell lines compared to the free drug.

## 2. Materials and methods

### 2.1. Live cell imaging

HEK293_$hY_1R$_eYFP, HEK293_HA_$hY_2R$_eYFP, HEK293_$hY_4R$_eYFP, HEK293_$hY_5R$_eYFP and MCF-7 cells were seeded into sterile μ-Slide 8 well plates (ibidi GmbH) and cultured for 24 h. For studies using bifluorescent ligands, HEK293 cells were seeded into μ-Slide 8 well plates, cultured for 24 h and transfected with the HA-$hY_1R$-pVitro2 vector using Lipofectamine™ (Invitrogen, Life Technologies; 1 μg DNA and 1 μl Lipofectamine™ per well, transfection for 60 min at 37 °C). Prior to ligand stimulation, cells were starved in OPTI-MEM® reduced serum medium (Gibco) for 30 min. Cell nuclei were imaged with Hoechst 33342 (0.5 mg/ml) nuclear stain. Stimulation occurred with 1 μM non-fluorescent peptide or 100 nM fluorescent peptide in OPTI-MEM® at 37 °C. For receptor internalization studies, images were taken after 60 min of stimulation. For studies using fluorescent peptides, stimulation occurred for 60 min, then cells were washed 3× with PBS (phosphate buffered saline, PAA/Lonza) and a further incubation period was performed in OPTI-MEM® for 60 min at 37 °C.

For tubulin destabilization studies, stable HEK293_$hY_1R$_eYFP and HEK293_HA_$hY_2R$_eYFP cells were stimulated with varying concentrations of cytolysin (**8**) or the cytolysin–[$F^7$,$P^{34}$]-NPY bioconjugate (**9**) for 16 h in standard growth medium. After treatment, nuclei were stained with Hoechst 33342 (0.5 mg/ml) for 30 min at 37 °C in Opti-MEM® reduced serum medium (Gibco). Subsequently, tubulin was stained with 2 μM SiR-tubulin (Spirochrome AG) per well for 2 h at 37 °C in Opti-MEM® reduced serum medium. 1 μM verapamil (efflux pump inhibitor) was added per well to improve tubulin staining.

Microscopy images were taken using an Axio Observer microscope equipped with an ApoTome imaging system (Zeiss). Image editing was performed with AxioVision software release 4.6.

### 2.2. Receptor binding studies

For competition binding assays, HEK293_$hY_1R$_eYFP cells were resuspended to a concentration of $6.25 \times 10^5$ cells/ml in DMEM/Ham's F-12 supplemented with 50 μM Pefabloc® SC (Fluka) and 1% BSA (*w*/*v*) (bovine serum albumin fraction V, PAA/Roth). In a 96-well plate $5 \times 10^4$ cells were incubated with $^{125}$I-PYY (Perkin Elmer) at a final concentration of 60 pM (in 1% BSA/bidest. $H_2O$ (*w*/*v*), calculated based on specific radioactivity, corresponds to $K_d$ [14]) and increasing concentrations of cold peptide (in 1% BSA/bidest. $H_2O$ (*w*/*v*)) for 60 min at room temperature under continuous shaking. Competition binding was terminated by filtration through a glass fiber filter Printed Filtermat B (Perkin Elmer) presoaked with 0.1% PEI (polyethylenimine in bidest. $H_2O$ (*v*/*v*), Fluka) using a FilterMate Harvester (Perkin Elmer). Filters were rapidly washed four times with ice-cold PBS and dried at 57 °C for 40 min in a hybridization oven/shaker (Amersham Pharmacia Biotech). Dried filters were sealed with melt-on scintillator sheets MeltiLex A (Perkin Elmer) and shrink-wrapped in sample bags for MicroBeta$^2$. Radioactivity was measured in a MicroBeta$^2$ Plate Counter (Perkin Elmer) and analyzed by GraphPad Prism 5.03 software. $IC_{50}$ values were calculated from sigmoidal concentration–response curves using non-linear regression curve fit with "log (inhibitor) vs. response (three parameters)" function. Experiments were performed in duplicate.

### 2.3. Receptor activation studies

For signal transduction (inositol phosphate (IP) accumulation) assays, COS-7_$hY_1R$_eYFP_$G\alpha_{\Delta 6qi4myr}$ and COS-7_$hY_2R$_eYFP_$G\alpha_{\Delta 6qi4myr}$ were seeded into 48-well plates and grown to confluency prior to labeling and stimulation. Labeling and stimulation were performed as described by Hofmann et al. [15]. Briefly, cells were labeled with 2 μCi/ml *myo*-[2-$^3$H(N)]-inositol (Perkin Elmer) 16 h prior to stimulation with peptide solution in concentration ranges from $10^{-5}$–$10^{-12}$ M in the presence of LiCl (lithium chloride, Sigma). Peptide stimulation was performed for 60 min. Intracellular IP species were isolated by anion exchange chromatography as described previously [16,17] and measured in a Tri-Carb 2910TR beta-counter (Perkin Elmer). Data were analyzed by GraphPad Prism 5.03 software and $EC_{50}$ values were calculated from concentration–response curves. Experiments were performed in duplicate.

### 2.4. Cell viability assay

For the fluorimetric resazurin-based cell viability assay (In Vitro Toxicology Assay Kit, Sigma-Aldrich), stable HEK293_$hY_1R$_eYFP, HEK293_HA_$hY_2R$_eYFP and human breast cancer cell lines were seeded in low densities into 96-well plates and were allowed to adhere for 24 h. Subsequently, increasing concentrations of cytolysin (**8**) and the cytolysin–[$F^7$,$P^{34}$]-NPY bioconjugate (**9**) were added to the cells. After 72 h under standard growth conditions, the incubation solution was replaced by 50 μl 10% resazurin solution in medium, and the cells were incubated for 2 h. Finally, the resorufin fluorescence by viable, metabolically active cells was measured using a Synergy 2 multi-mode microplate reader (BioTek) with 540 nm excitation and 590 nm emission filter setting. Experiments were performed in triplicate.

### 2.5. Caspase assays

For the luminescent caspase assays (Promega GmbH), breast cancer cell lines were seeded into 96-well plates and were allowed to adhere for 24 h. Subsequently, 1 μM cytolysin–[$F^7$,$P^{34}$]-NPY bioconjugate (**9**) dissolved in medium was added to the cells. Cells were incubated for 16–48 h under standard growth conditions. For the last hour of incubation, 10 μl/well of 8× resazurin solution (400 μM) were added in order to multiplex the caspase activities with the cell number/cell viability. When the incubation was finished, the resorufin fluorescence was measured as described above. After that, Caspase-Glo® assay reagent (Promega GmbH) was added according to Promega's guidelines and incubated for 1 h at room temperature. Luminescence read-out was performed using a Synergy 2 multi-mode microplate reader (BioTek).

### 2.6. SILAC labeling and treatment of cells

MCF-7 and MDA-MB-468 cells were cultivated in lysine and arginine-depleted DMEM/Ham's F-12 and RPMI 1640 (PAA), respectively. The medium was supplemented with 10% (*v*/*v*) dialyzed, heat-inactivated FCS, 3.15 g/l glucose, 2 mM L-glutamine (Invitrogen, Life Technologies) and 200 mg/l L-proline (Thermo Fisher Scientific) to prevent labeled arginine-to-proline conversion. RPMI 1640 medium was additionally

supplemented with 0.01 mg/l insulin (Roche). Cells were grown under standard conditions but in the presence of $^{12}C_6$-L-arginine and $^{12}C_6$-L-lysine for light conditions, $^{13}C_6$-L-arginine and $^{2}H_4$-L-lysine for medium conditions and $^{13}C_6$,$^{15}N_4$-L-arginine and $^{13}C_6$,$^{15}N_2$-L-lysine (Thermo Fisher Scientific) for heavy conditions for 9 days prior to treatment, to allow complete metabolic incorporation of the isotopic amino acids. For treatment, cells were starved for 30 min in SILAC medium without additives and subsequently cultivated for 24 h in complemented SILAC medium, supplemented with 100 nM cytolysin (**8**) and 1 μM cytolysin–[F$^7$,P$^{34}$]-NPY bioconjugate (**9**), respectively. Experiments were performed in six biological replicates and each treatment as well as the control was performed under light, medium and heavy conditions (label-swap). For sample preparation, liquid chromatography tandem mass spectrometry and data analysis see Supplementary methods.

### 2.7. Statistical analysis

For SILAC experiments a conservative SILAC-ratio of 1.5-fold increase or 0.7-fold decrease in protein abundance above/below basal level with a p-value (Student's *t*-test, two-tailed, assuming unequal variance) $\leq 0.05$ was considered as significant.

Nonlinear regression, sigmoidal concentration-response fitting as well as calculations of means, SEM and statistical analyses were performed using the GraphPad Prism 5.03 software. Significances were calculated by ANOVA and Dunnett's post-hoc test with $^{*}p \leq 0.05$, $^{**}p \leq 0.01$.

## 3. Results and discussion

### 3.1. Monitoring the release of a disulfide-linked cargo after $hY_1R$ internalization

The human $Y_1$-receptor ($hY_1R$) is known to internalize after ligand binding and signal transduction into endosomes [18]. The use of the $hY_1R$-preferring derivative [F$^7$,P$^{34}$]-neuropeptide Y (NPY) as a shuttle system to transport toxic cargo molecules into cells requires the intracellular release of these molecules to exert their specific action [3]. In order to monitor this release, instead of a toxic molecule, the fluorescent label *TAMRA* was coupled either by an amide linker (**1**) or a disulfide linker (**2**) to the N$^{\varepsilon}$-amino group of lysine residue 4 (Lys$^4$) of an N-terminally *CF*-labeled [F$^7$,P$^{34}$]-NPY (Table 1). Both positions are described to be insensitive to modifications regarding receptor binding and activation [12,19]. In subsequent fluorescent live-cell microscopy studies, HEK293 cells transiently transfected with the $hY_1R$ were stimulated with either 100 nM of peptide (**1**) or (**2**). Both peptides showed an identical and clear internalization pattern after 60 min of stimulation, with vesicles containing the *TAMRA*- and the *CF*-fluorophore (Fig. 1). After washing the cells and recycling for 60 min, for peptide (**1**) the amide-linked *TAMRA* and *CF* were still visible inside vesicles, however, for peptide (**2**) only the amide-linked *CF* was still detectable, while the disulfide-linked *TAMRA* was no longer observed. This observation allowed for the conclusion that only the disulfide linker is cleaved in the endosomes releasing the *TAMRA*-fluorophore into the cytosol and thereby preventing its detection by fluorescence microscopy. Inside endosomes the concentration of fluorescent peptides is assumed to be very high and therefore the fluorophores can be easily detected by fluorescence microscopy. However, if a fluorophore is cleaved off a peptide and translocated into the cytoplasm, it will be distributed into a much larger space and thus, its concentration will decrease abruptly preventing its detection in the fluorescence microscope [20,21]. Although the amide linker is described as an enzyme-cleavable linker [22], under the relevant conditions it seemed to be stable and therefore not suitable for cargo-release inside the cell. The disulfide linker, described to be chemically labile and cleaved by reduction [22], showed a fast intracellular cleavage in endosomal and lysosomal compartments.

The selective cleavage of the disulfide linker was additionally tested with the labeled peptide [K$^4$(Ac-C(*TAMRA*)),F$^7$,P$^{34}$]-NPY (**3**) (Table 1) in HEK293 cells stably expressing $hY_1R$ or $hY_2R$ C-terminally fused to the enhanced yellow fluorescent protein (eYFP) (Supplementary Fig. 1a, b). While the *TAMRA*-fluorescence decreased in HEK293_$hY_1R$_eYFP cells after recycling, in HEK293_HA_$hY_2R$_eYFP cells no internalization of the $hY_1R$-preferring peptide (**3**) was visible. Finally, linker cleavage was also analyzed in the breast cancer cell line MCF-7, endogenously expressing the $hY_1R$ [23] (Supplementary Fig. 1c). The cells showed internalization of the peptide (**3**) as well as disappearance of *TAMRA*-fluorescence after recycling, confirming the disulfide bond cleavage.

Accordingly, the disulfide linker was chosen to connect the $hY_1R$-preferring precursor peptide [K$^4$(βA-C),F$^7$,P$^{34}$]-NPY (**7**) and the cytolysin (**8**) (Table 1, Supplementary Scheme 1). Identity and purity of the novel bioconjugate (**9**) were determined by MALDI- and ESI-mass spectrometry and RP-HPLC (Table 1, Supplementary Fig. 2). The successful release of cytolysin from [K$^4$(βA-C),F$^7$,P$^{34}$]-NPY (**7**) was demonstrated in vitro by incubating the cytolysin–[F$^7$,P$^{34}$]-NPY bioconjugate (**9**) with the natural reducing agent glutathione (GSH) (Supplementary Fig. 3).

### 3.2. In vitro characterization of the cytolysin–[F$^7$,P$^{34}$]-NPY bioconjugate

Conjugating a peptide with a toxic molecule always bears the risk of losing the targeting characteristics of the peptide, i.e. binding, activating and foremost internalizing properties [24]. To confirm that the coupling of the cytolysin (**8**) did not alter the peptide regarding receptor binding and selective activation, $^{125}$I-PYY displacement assays and *myo*-[2-$^{3}$H(N)]-inositol phosphate accumulation assays were performed, respectively (Fig. 2a–c). Binding assays revealed a slight shift in affinity of

**Table 1**
Analytical characterization of synthesized peptides. Peptides were identified by MALDI-mass spectrometry. Cytolysin-dithiopyridine (**8**) was identified by ESI-mass spectrometry.

| No. | Compound | MALDI-ToF MS | | RP-HPLC retention time [min] | | Purity [%][i] |
|---|---|---|---|---|---|---|
| | | $M_{calc.}$ [Da][a] | $M_{obs.}$ [Da][b] | $C_{18}$ 90 Å | Polym. 200 Å | |
| (**1**) | *CF*-[K$^4$(*TAMRA*),F$^7$,P$^{34}$]-NPY | 5023.3 | 5024.3 | 31.3[c] | 27.0[d] | 94 |
| (**2**) | *CF*-[K$^4$(Ac-C(*TAMRA*)),F$^7$,P$^{34}$]-NPY | 5243.4 | 5244.2 | 32.2[c] | 27.8[d] | >95 |
| (**3**) | [K$^4$(Ac-C(*TAMRA*)),F$^7$,P$^{34}$]-NPY | 4885.3 | 4886.5 | 27.4[c] | 24.7[d] | >95 |
| (**4**) | NPY | 4251.1 | 4252.1 | 23.4[c] | 18.9[d] | 93 |
| (**5**) | hPP | 4179.1 | 4180.2 | 23.6[c] | 18.9[d] | 94 |
| (**6**) | [F$^7$,P$^{34}$]-NPY | 4253.1 | 4254.2 | 24.5[c] | 20.2[d] | >95 |
| (**7**) | [K$^4$(βA-C),F$^7$,P$^{34}$]-NPY | 4427.2 | 4428.2 | 24.5[c] | 18.4[f] | >95 |
| (**8**) | Cytolysin-dithiopyridine | 942.3 | 942.4 | 36.0[e] | 27.9[f] | >95 |
| (**9**) | [K$^4$(βA-C(**8**)),F$^7$,P$^{34}$]-NPY | 5257.6 | 5258.7 | 24.6[e] | 25.7[f] | >95 |
| (**10**) | *TAMRA*-[F$^7$,P$^{34}$]-NPY | 4665.3 | 4666.2 | 27.3[c] | 23.7[d] | >95 |
| (**11**) | *TAMRA*-[K$^4$(βA-C(**8**)),F$^7$,P$^{34}$]-NPY | 5669.8 | 5670.7 | 29.6[c] | 26.7[d] | >95 |
| (**12**) | *TAMRA*-[K$^4$(βA-C(**8**)-PAM),F$^7$,P$^{34}$]-NPY | 5907.8 | 5908.9 | 41.5[g] | 37.5[h] | >95 |

*CF*: 5(-6)-carboxyfluorescein; *TAMRA*: 5(-6)-carboxytetramethylrhodamine; PAM: palmitic acid; a) $M_{calc.}$: calculated mass in Dalton. b) $M_{obs.}$: observed mass in Dalton (corresponds to molecule ion peaks $[M+H]^+$). c–h) Retention times using a Jupiter 4 μ Proteo $C_{18}$, 90 Å or a VariTide RPC, 200 Å column with linear gradients of 20–60% (v/v) eluent B in eluent A in 40 min (c, d), 20–70% (v/v) eluent B in eluent A in 40 min (e, f) or 20–80% (v/v) eluent B in A in 60 min (g, h). i) Purity was quantified by RP-HPLC using two different columns.

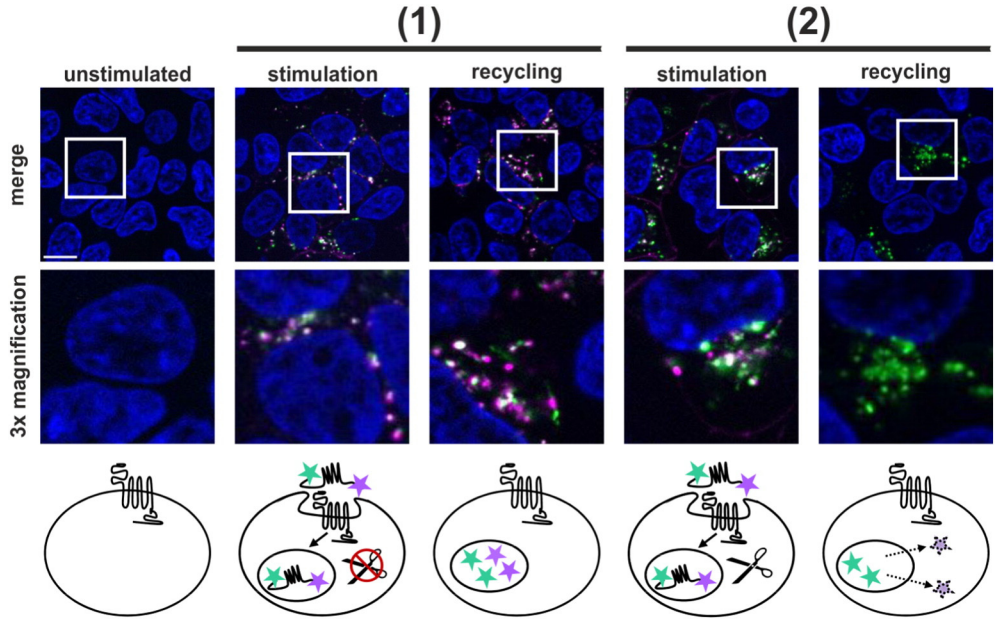


**Fig. 1.** Disulfide bonds are cleaved after internalization. In peptide (**1**) both fluorophores *TAMRA* (magenta) and *CF* (green) are connected to the peptide via amide bonds. In peptide (**2**) *CF* is connected to the peptide via an amide bond, while *TAMRA* is coupled to the peptide using a disulfide bond. Nuclei are stained in blue. Pictures are representative for ≥3 experiments. Scale bar: 10 μm.

the cytolysin–[$F^7$,$P^{34}$]-NPY bioconjugate (**9**) ($IC_{50}$: 47.6 nM) compared to the natural ligand NPY (**4**) ($IC_{50}$: 1.8 nM) and the lead peptide [$F^7$,$P^{34}$]-NPY (**6**) ($IC_{50}$: 1.3 nM) (Fig. 2a). However, receptor activation studies verified the maintained ability to fully activate the $hY_1R$ and exhibited $EC_{50}$ values in the low nanomolar range for all three peptides (Fig. 2b). At the $hY_2R$, NPY (**4**) induced receptor activation with an $EC_{50}$ value of 0.4 nM, while the $hY_1R$-preferring peptides (**6**) and (**9**) led to a clear rightwards shift of the concentration-response curves, demonstrating a maintained preference over $hY_2R$ also for the bioconjugate (Fig. 2c).

### 3.3. Selective $hY_1R$ internalization and toxic effect after treatment with the cytolysin–[$F^7$,$P^{34}$]-NPY bioconjugate

To ensure selective internalization of the cytolysin–[$F^7$,$P^{34}$]-NPY bioconjugate (**9**) by $hY_1R$-mediated endocytosis, internalization studies were performed with HEK293 cells, stably transfected with either of the hYR subtypes fused to eYFP (Fig. 2d). The yellow fluorescent receptor fusion protein was located in the cell membrane, while fluorescence visible inside the cytoplasm was probably due to receptor biosynthesis and degradation steps [25]. Stimulation of the receptors for 60 min with 1 μM of the natural ligands NPY (**4**) for $hY_1R$, $hY_2R$ and $hY_5R$ and hPP (**5**) for $hY_4R$ led to a clear internalization of $hY_1R$, $hY_2R$ and $hY_4R$ as can be seen by fluorescent intracellular vesicles. $hY_5R$ internalized very slowly and in only low amounts hardly visible after 60 min, as described previously [18]. Stimulation with the $hY_1R$-preferring peptide [$F^7$,$P^{34}$]-NPY (**6**) only showed clear internalization into intracellular vesicles of the $hY_1R$, but no internalization of the $hY_2R$, $hY_4R$ and $hY_5R$ was observed, with the receptors still being localized in the cell membrane comparable to unstimulated cells. The internalization profile of the cytolysin–[$F^7$,$P^{34}$]-NPY bioconjugate (**9**) was comparable to [$F^7$,$P^{34}$]-NPY (**6**), confirming the maintained $hY_1R$ preference.

In order to demonstrate the specific toxic effect of the cytolysin–[$F^7$,-$P^{34}$]-NPY bioconjugate (**9**), cytotoxicity assays were performed with stable HEK293_$hY_1R$_eYFP and HEK293_HA_$hY_2R$_eYFP cells which were treated either with 50 nM cytolysin (**8**) or increasing concentrations of the cytolysin–[$F^7$,$P^{34}$]-NPY bioconjugate (**9**) (Fig. 2e). While the cytolysin (**8**) treatment induced cytotoxicity in both HEK293_$hY_1R$_eYFP and HEK293_HA_$hY_2R$_eYFP cells, the cytolysin–[$F^7$,$P^{34}$]-NPY bioconjugate (**9**) elicited a significant toxic effect only in $hY_1R$-expressing cells.

Therefore, the cytolysin–[$F^7$,$P^{34}$]-NPY bioconjugate can be considered as a potent peptide–drug shuttle, selectively targeting $hY_1R$-expressing breast cancer cells and yet not affecting $hY_2R$-expressing healthy tissue cells [8].

### 3.4. Selective destabilization of the tubulin network after treatment with the cytolysin–[$F^7$,$P^{34}$]-NPY bioconjugate

The cytolysin coupled to [$F^7$,$P^{34}$]-NPY is a chemical derivative of the myxobacterial tubulysins, a family of natural tetrapeptides [26]. Tubulysins themselves are highly promising chemotherapeutics characterized by a high cytotoxic activity inhibiting the microtubule polymerization followed by $G_2$/M cell cycle arrest and eventually cellular death [27]. To investigate the effect of cytolysin (**8**) and the cytolysin–[$F^7$,$P^{34}$]-NPY bioconjugate (**9**) on the tubulin network integrity, stable HEK293_$hY_1R$_eYFP as well as HEK293_HA_$hY_2R$_eYFP cells were treated with varying concentrations of the compounds for 16 h. After treatment, tubulin was labeled by a silicon–rhodamine (SiR)-derived, fluorogenic probe [28] and nuclei were stained with Hoechst 33342 to visualize possible nuclei fragmentation as a sign of apoptosis [29]. While non-treated cells showed intact tubulin network and nuclei, treatment with 50 nM of cytolysin (**8**) and 100 nM of the bioconjugate (**9**) caused a disruption of the tubulin network indicated by decreased and blurred tubulin staining as well as nuclei fragmentation and an altered cell morphology (Fig. 3).

To verify, that no undesired premature release of the cytolysin took place before entering the cell, stability of the cytolysin–[$F^7$,$P^{34}$]-NPY bioconjugate (**9**) was tested under different conditions and analyzed by ESI-mass spectrometry (Supplementary Fig. 4). The bioconjugate showed high stability in sodium acetate buffer (pH 4) over 24 h without formation of cleavage products (Supplementary Fig. 4a). Also in cell culture supernatant of MCF-7 cells no cleavage was detected within 24 h, confirming the necessary stability for subsequent treatments of breast cancer cell lines (Supplementary Fig. 4b). Release of the cytolysin was achieved only under reductive conditions (20× cysteine, pH 6.0) (Supplementary Fig. 4c).

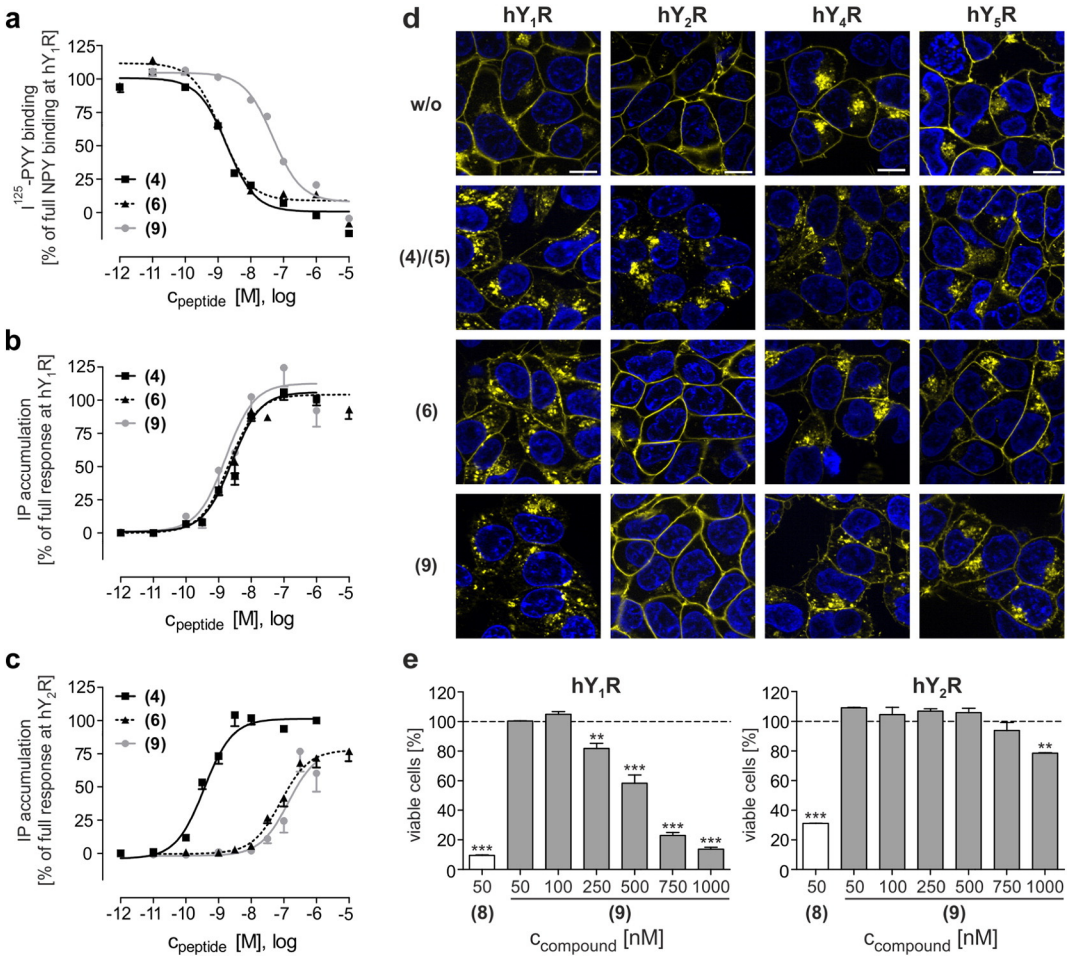


**Fig. 2.** Cytolysin–[F$^7$,P$^{34}$]-NPY bioconjugate (**9**) activates the hY$_1$R and induces selective receptor internalization and toxicity. (a) $^{125}$I-PYY displacement assays reveal a shift in binding affinity at hY$_1$R of (**9**) (IC$_{50}$: 47.6 nM) compared to (**4**) (IC$_{50}$: 1.8 nM) and (**6**) (IC$_{50}$: 1.3 nM). (b) The concentration–response curve at the hY$_1$R for (**9**) (EC$_{50}$: 1.7 nM) is in the same range as for (**4**) (EC$_{50}$: 2.6 nM) and (**6**) (EC$_{50}$: 2.1 nM). (c) The concentration–response curve at the hY$_2$R for (**4**) leads to an EC$_{50}$ value in the low nanomolar range (EC$_{50}$: 0.4 nM). In contrast, (**6**) and (**9**) exhibit an EC$_{50}$ shift and are not able to fully activate the hY$_2$R. Values are mean ± SEM of ≥2 experiments. (d) Internalization studies show cell membrane localization of all hYR subtypes (yellow) in the native state (upper panel). Stimulation with 1 μM of peptides (**4**), (**5**), (**6**) and (**9**) was performed for 60 min. Nuclei are stained in blue. Pictures are representative for ≥3 experiments. Scale bar: 10 μm. (e) For cell viability studies, stable HEK293_hY$_1$R_eYFP and HEK293_HA_hY$_2$R_eYFP cells were treated with 50 nM (**8**) or increasing concentrations of (**9**) for 24 h at 37 °C. After 72 h under standard growth conditions, cell viability was determined by resazurin assay. Bars represent mean ± SEM of two independent experiments. Measurements were normalized by using only medium treated cells (set at 100%) and ethanol treated cells (set at 0%). Statistical significance refers to only medium treated cells and was determined by one-way ANOVA followed by Dunnett's multiple comparison test. $^{**}p < 0.01$, $^{***}p < 0.001$.

Thus, the general tubulysin-like activity of the conjugated cytolysin was proven, showing that [F$^7$,P$^{34}$]-NPY successfully delivers and releases the active cargo to its required site of action. Once the general requirements for a novel PDC were given, in-depth analyses of its function were pursued in cellular model systems for breast cancer.

### *3.5. Cytostatic and cytotoxic effect of the cytolysin–[F$^7$,P$^{34}$]-NPY bioconjugate in breast cancer cell lines MCF-7 and MDA-MB-468*

Two human-derived breast cancer cell lines, predominantly used in research, were chosen for further investigations [30]. MCF-7 as estrogen-receptor (ER)-positive cells [31], which are often successfully treated with chemotherapy and MDA-MB-468 as triple-negative cells, demonstrating enhanced malignant/metastatic behavior and poor treatment prognosis [32,33]. Both cell lines are described to express the hY$_1$R [23,34] and extraction of mRNA and subsequent quantitative real-time PCR experiments confirmed hY$_1$R-expression, with a higher level of receptor-mRNA observed in MCF-7 compared to MDA-MB-468 cells (Supplementary Fig. 5).

To investigate cytostatic and cytotoxic effects of the free cytolysin (**8**) and the cytolysin–[F$^7$,P$^{34}$]-NPY bioconjugate (**9**), proliferation assays were performed, treating the breast cancer cell lines with different compound concentrations over 72 h (Fig. 4a). The IC$_{50}$ values for the free cytolysin (**8**) (MCF-7 IC$_{50}$: 18.4 nM; MDA-MB-468 IC$_{50}$: 17.4 nM) were comparable in both cell lines and for the cytolysin–[F$^7$,P$^{34}$]-NPY bioconjugate (**9**) (MCF-7 IC$_{50}$: 405.3 nM; MDA-MB-468 IC$_{50}$: 236.1 nM) a ~10-fold decrease was observed, since for the bioconjugate the delivery via the receptor is the limiting factor. Furthermore in MDA-MB-468 high concentrations of cytolysin (**8**) and the cytolysin–[F$^7$,P$^{34}$]-NPY bioconjugate (**9**) resulted in full loss of cell viability, indicating a cytotoxic effect of the compounds. However in MCF-7 even with high compound concentrations around 25% cells remained viable, pointing to a cell growth arrest and therefore a cytostatic effect. It was previously described, that anti-proliferative and pro-apoptotic actions can depend on drug concentration [35] as well as on the genetic makeup [36,37]. In contrast to MDA-MB-468, MCF-7 cells are described to lack caspase-3 [38], which shows high importance during the terminal or demolition phase of apoptosis [39,40]. To examine a possible involvement of apoptotic mechanisms, the activation of caspases-3, -7 and -9 by the cytolysin–[F$^7$,P$^{34}$]-NPY bioconjugate (**9**) was determined (Fig. 4b, c). MCF-7 and MDA-MB-468 were treated with 1 μM of the bioconjugate (**9**) for up to 48 h. While MCF-7 neither showed caspase-3/7 nor caspase-9 activation over the entire treatment period, in MDA-MB-468, however, an activation of all three caspases was detected. Thus,

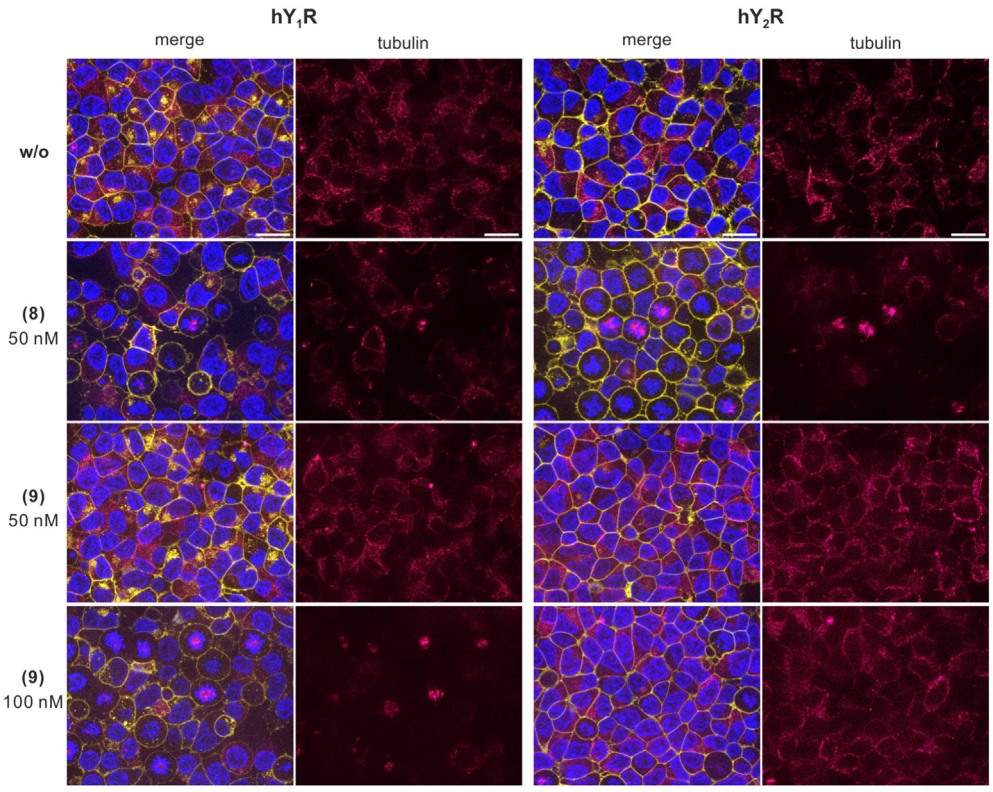


**Fig. 3.** Cytolysin–[F$^{7}$,P$^{34}$]-NPY bioconjugate (**9**) induces selective tubulin degradation and nuclei fragmentation. Stable HEK293_hY$_1$R_eYFP and HEK293_HA_hY$_2$R_eYFP cells were treated with cytolysin (**8**) and cytolysin–[F$^{7}$,P$^{34}$]-NPY bioconjugate (**9**) for 16 h at 37 °C in standard growth medium. Subsequently, nuclei were stained with Hoechst 33342 (blue) and tubulin was visualized by the live cell fluorogenic microtubule labeling probe SiR tubulin (red). Representative pictures of ≥2 independent experiments are shown. Scale bar: 20 μm.

in MDA-MB-468 cells the cytotoxic effect of cytolysin (**8**) and the cytolysin–[F$^{7}$,P$^{34}$]-NPY bioconjugate (**9**) is confirmed by an induction of caspase-related apoptotic pathways.

The toxic effect of the free cytolysin (**8**) as well as the cytolysin–[F$^{7}$,-P$^{34}$]-NPY bioconjugate (**9**) was furthermore demonstrated in two additional breast cancer cell lines T-47D (ER-positive) and MDA-MB-231 (triple negative) confirming the observations made with MCF-7 and MDA-MB-468 (Supplementary Fig. 6).

### *3.6. Identical mode of action of free cytolysin and the cytolysin–[F$^{7}$,P$^{34}$]-NPY bioconjugate in adherent MCF-7 and MDA-MB-468 cells confirmed by triple SILAC*

Although the described experiments point to the fact, that the cytolysin conjugated to [F$^{7}$,P$^{34}$]-NPY is still active similar to the free compound, this is only a general view from above. In order to confidently determine that the peptide–drug shuttle does not lead to additional alterations in cellular protein composition owing to the agonistic activity of the peptide compared to treatment with the sole chemotherapeutic, thorough proteomic analyses are necessary [41]. Therefore, a triple SILAC approach coupled to LC–MS/MS analysis was applied, enabling the direct comparison of protein regulations in two differently treated cell populations versus untreated cells. Heavy-, medium- and light-labeled MCF-7 and MDA-MB-468 cells were cultivated with either 100 nM free cytolysin (**8**), 1 μM bioconjugate (**9**) or standard SILAC-culture medium. Since cells gradually detached from the surface during treatment, detached cells were separated from adherent cells to evaluate protein regulations in both cell states in comparison to the untreated control. In adherent MCF-7 and MDA-MB-468 cells in total 1153 and 1297 proteins were quantified, respectively, with up to 12 upregulations and 5 downregulations (Supplementary Fig. 7). Classification of the upregulated proteins showed that a majority is involved in the cell cycle (Table 2) with stronger regulations in MCF-7 than in MDA-MB-468 cells, as is also shown for selected proteins in Western blot analyses

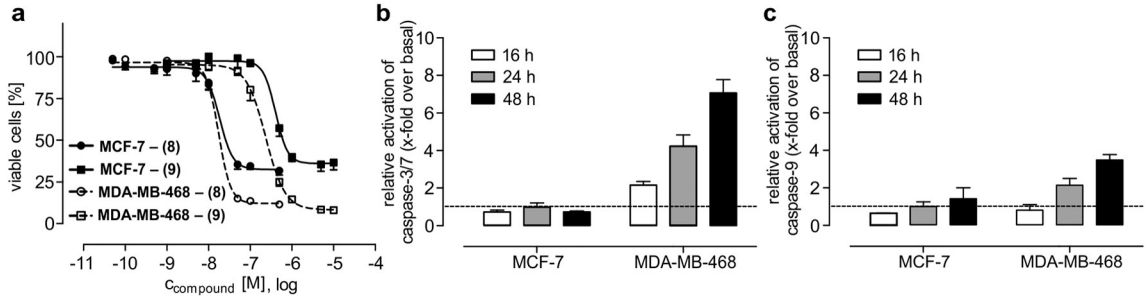


**Fig. 4.** Cytolysin (**8**) and cytolysin–[F$^{7}$,P$^{34}$]-NPY bioconjugate (**9**) induce a cytostatic effect in MCF-7 cells and a cytotoxic effect in MDA-MB-468 cells. (a) For proliferation analysis MCF-7 and MDA-MB-468 cells were treated with different concentrations of (**8**) and (**9**) for 72 h. Cell viability was determined by resazurin assay. Values are mean ± SEM of ≥3 experiments. (b, c) For assessment of caspases-3/7 and -9 activation, MCF-7 and MDA-MB-468 cells were treated with 1 μM of (**9**) for up to 48 h. Data are normalized to the cell number and are expressed as relative activities, i.e. x-fold over medium-treated cells (basal).

(Supplementary Fig. 8). Especially the stronger regulated proteins such as kinesin-like protein KIF20A, kinesin-like protein KIFC1 and importin subunit alpha-2 (Table 2, Supplementary Fig. 8) are described as being essential in the $G_2$- and early M-phase of the cell cycle [42–44] either necessary for spindle formation or as nuclear import transporter of cell cycle checkpoint mediators [45]. As described for tubulysin, these results confirm that cytolysin also induces a $G_2$/M-phase arrest in MCF-7 cells [27]. Adherent MDA-MB-468 cells rather being affected in a cytotoxic manner, expectably showed less regulation of proteins involved in cell cycle. In MDA-MB-468 cells additional proteins are involved in cell communication, cell adhesion, actin cytoskeleton and primary metabolic processes mainly pointing to cytoskeleton reorganization and changes in cell communication and cell adhesion (Table 2) as early signs for rounding of cells and detachment [46]. This detachment process is described as an early stage of apoptosis [47] involving the caspase-dependent degradation of cell–cell adhesion complexes, which is in complete agreement with caspase-3/7 and -9 induction measured in the performed caspase-assays (Fig. 4b, c).

The proteomic analysis in adherent cells enabled a deeper insight into molecular mechanisms thereby allowing the confirmation of the tubulysin-like effect of the cytolysin and giving a more extensive explanation for the different responses of the two cell lines MCF-7 and MDA-MB-468. However, more importantly, looking at the specific SILAC-ratios in cytolysin- and cytolysin–[$F^7$,$P^{34}$]-NPY bioconjugate-treated cells (Table 2), it became obvious, that regardless of the route of delivery, both treatments resulted in almost identical protein regulations, even displaying the cell line specific differences. The proceeding analyses of the detached cells then even further reinforced the above mentioned conclusion.

### 3.7. Triple SILAC analysis of detached MCF-7 and MDA-MB-468 cells reveals protein regulations mainly in cellular and metabolic processes

Detached cells were also compared to untreated adherent cells. In detached MCF-7 and MDA-MB-468 cells in total 1053 and 1466 proteins were quantified, respectively (Supplementary Fig. 9). Here up to 15 upregulations and 54 downregulations were observed. While the adherent cells showed only few protein upregulations, in detached cells, possibly representing early stages of apoptosis [47], predominantly a reduction of protein abundance was observed. The regulated proteins were mainly categorized into five categories (cellular process, metabolic process, cellular component organization, developmental process and localization) (Fig. 5). This categorization gave an identical distribution pattern for both treatments (Fig. 5a, b, Supplementary Table 1 + 2) with mainly cellular and metabolic processes being influenced. Interestingly, also in detached cells, cell line specific differences could be observed in upregulated proteins. While in detached MCF-7 cells more regulated proteins were assigned to the localization-category, in detached MDA-MB-468 cells proteins in developmental processes were upregulated. Since even these cell line specific differences can be observed in both treatments, we can state an identical mode of action for the cytolysin conjugated to the [$F^7$,$P^{34}$]-NPY compared to the free cytolysin.

As a first step towards an in vivo application of this novel PDC, stability assays were performed in human blood plasma with N-terminally *TAMRA*-modified analogs (Table 1), which enable the monitoring of possible peptide degradation and the identification of potential cleavage products (Supplementary Fig. 10). The peptide *TAMRA*-[$K^4$(βA-C(**8**)),$F^7$,$P^{34}$]-NPY (**11**) revealed a half-life of 168 ± 48 min, which is comparable to other PDCs that are currently evaluated in clinical trials [48–50]. Furthermore, the possibility of additionally stabilizing the PDC was analyzed by incorporation of palmitic acid (PAM) adjacent to the disulfide bridge, since lipidation is described to prolong the in vivo half-life [3]. Additionally, the derivatization of peptides with palmitic acid may enhance the rate of receptor internalization [51], which would be beneficial for drug delivery to breast cancer cells. The peptide analog *TAMRA*-[$K^4$(βA-C(**8**)-PAM),$F^7$,$P^{34}$]-NPY (**12**) showed an increased half-life in human blood plasma of 144 ± 22 h (Supplementary Fig. 10) making palmitoylation a promising stabilization method for future peptide–drug conjugates.

## 4. Conclusion

In conclusion, here the synthesis of a novel, selective and highly active PDC is described. The $hY_1R$-preferring peptide [$F^7$,$P^{34}$]-NPY is conjugated with a toxic cytolysin using a disulfide bond. While the peptide enables the selective targeting of the $hY_1R$ overexpressed in breast cancer cells, internalization of the bioconjugate–receptor complex permits precise delivery of the coupled toxin, and efficient cleavage of the labile

**Table 2**
SILAC-ratios and functions of regulated proteins detected in adherent MCF-7 and adherent MDA-MB-468 cells by triple SILAC experiment. Protein identification and SILAC-ratios were determined by MaxQuant analysis (version 1.2.2.5). Statistical analysis was performed using Student's *t*-test. Gene ontology categorization is based on information provided by the online resource PANTHER 9.0 classification system.

| Protein name | Accession number (UniProt) | SILAC-ratio treated/untreated[a] ± SEM[b] (n) | | | | GO term name (GO identifier) |
|---|---|---|---|---|---|---|
| | | MCF-7 | | MDA-MB-468 | | |
| | | Cytolysin (**8**) | Cytolysin–[$F^7$,$P^{34}$]-NPY (**9**) | Cytolysin (**8**) | Cytolysin–[$F^7$,$P^{34}$]-NPY (**9**) | |
| Cytoskeleton-associated protein 5 | Q14008 | 1.6 ± 0.2 (6) | 1.5 ± 0.2 (6) | n.r. [1.3 (6)] | n.r./n.s. | Cell cycle (GO:0007049) |
| Ubiquitin-conjugating enzyme E2C | O00762 | 1.6 ± 0.1 (4) | 1.5 ± 0.1 (4) | 1.5 ± 0.2 (4) | 1.6 ± 0.1 (4) | |
| Ubiquitin-conjugating enzyme E2S | Q16763 | n.i. | n.i. | 2.5 ± 0.3 (3) | 2.0 ± 0.3 (3) | |
| DNA topoisomerase 2-alpha | P11388 | 2.1 ± 0.1 (6) | 2.0 ± 0.1 (6) | 1.8 ± 0.1 (5) | 1.6 ± 0.2 (5) | |
| Kinesin-like protein KIFC1 | Q9BW19 | 2.7 ± 0.5 (3) | 2.2 ± 0.3 (3) | n.i. | n.i. | |
| Importin subunit alpha-2 | P52292 | 3.7 ± 0.2 (6) | 3.4 ± 0.3 (6) | 1.8 ± 0.05 (6) | 1.7 ± 0.1 (6) | |
| Kinesin-like protein KIF20A | O95235 | 5.7 ± 0.2 (6) | 4.6 ± 0.4 (6) | 2.3 ± 0.1 (4) | 1.6 ± 0.1 (4) | |
| G2/mitotic-specific cyclin-B1 | P14635 | n.s. [2.1 (2)] | 2.7 ± 0.03 (2) | n.q. | n.q. | |
| Actin-binding protein anillin | Q9NQW6 | n.i. | n.i. | 2.3 ± 0.3 (4) | 2.7 ± 0.3 (5) | Cell communication (GO:0007154) |
| Protein CYR61 | O00622 | n.i. | n.i. | 3.1 ± 0.2 (5) | 6.1 ± 0.7 (5) | |
| Intercellular adhesion molecule 1 | P05362 | n.i. | n.i. | n.r./n.s. | 1.6 ± 0.1 (6) | Cell adhesion (GO:0007155) |
| Palladin | Q8WX93 | n.i. | n.i. | n.s. [2.1 (4)] | 1.8 ± 0.2 (4) | |
| Transgelin | Q01995 | n.i. | n.i. | 2.7 ± 0.6 (5) | 4.0 ± 1.4 (5) | Actin cytoskeleton (GO:0015629) |
| Cysteine and glycine-rich protein 1 | P21291 | n.r./n.s. | n.r. [1.0 (3)] | 1.5 ± 0.1 (5) | 1.7 ± 0.2 (5) | |
| Ribonucleoside-diphosphate reductase | P31350 | n.q. | n.q. | n.r. [1.4 (5)] | 1.6 ± 0.02 (5) | Primary metabolic process (GO:0044238) |

SEM: standard error of the mean; n.i.: not identified; n.q.: not quantified; n.r.: not regulated [ratio (n)] (ratio < 1.5); n.s. = not significant [ratio (n)] ($p > 0.05$).
[a] SILAC-ratios represent protein regulations of treated to untreated protein amounts; a conservative ratio of 1.5-fold increase or 0.7-fold decrease in protein abundance compared to the basal level with $p \leq 0.05$ was considered significant.
[b] Values are given as mean ± SEM.

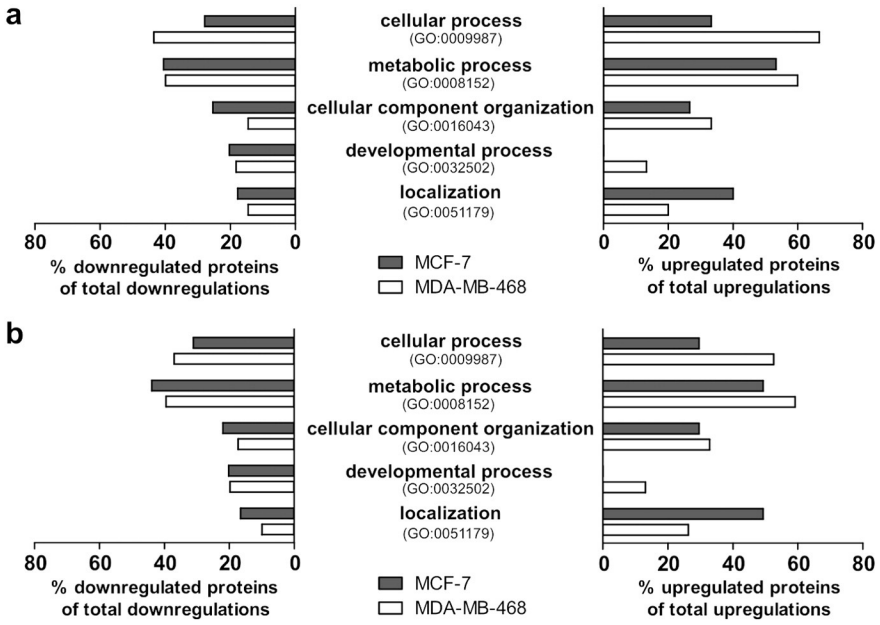


**Fig. 5.** Categorization of regulated proteins in detached cells indicates that cytolysin (**8**) as well as cytolysin–[$F^7$,$P^{34}$]-NPY bioconjugate (**9**) treatment mainly influence cellular and metabolic processes. Protein identification and quantification were determined by MaxQuant analysis (version 1.2.2.5). Gene ontology categorization (GO) is based on information provided by the online resource PANTHER 9.0 classification system. (a) Categorization of upregulated and downregulated proteins in cytolysin (**8**)-treated MCF-7 and MDA-MB-468 cells. (b) Categorization of upregulated and downregulated proteins in cytolysin–[$F^7$,$P^{34}$]-NPY bioconjugate (**9**)-treated MCF-7 and MDA-MB-468 cells.

disulfide linker inside the endosomes of the tumor cell releases the cytolysin into the cytoplasm. Finally, in-depth proteomic analyses revealed an identical mode of action of the conjugated cytolysin compared to the free drug in ER-positive as well as triple negative breast cancer cell line models. These new findings introduce a capable peptide–drug shuttle system with promising prospects for a targeted and personalized cancer therapy featuring the molecular medicine of the future.

## Competing financial interests

The authors declare no competing financial interests.

## Acknowledgments

The authors gratefully acknowledge the financial support of the Federal Ministry of Education and Research (BMBF, 0315919A/031519B) and the State of Saxony and the European Union (ESF 22117016). V.M. Ahrens and D. Böhme express their thanks for the financial support of the graduate school "Leipzig School of Natural Sciences — Building with Molecules and Nano-objects" (BuildMoNa). K.B. Kostelnik gratefully acknowledges financial contribution of the graduate school "Helmholtz Interdisciplinary GRADuate School for Environmental Research" (HIGRADE). S. Kalkhof and M. von Bergen are thankful for partial financial support by SFB TR 67. The authors would also like to thank Regina Reppich, Kristin Löbner and Janine Ulrich for excellent assistance in mass spectrometry, cell culture and screening, as well as Dr. Sven Baumann for support at the Helmholtz Centre for Environmental Research (UFZ).

## Appendix A. Supplementary data

Supplementary data to this article can be found online at http://dx.doi.org/10.1016/j.jconrel.2015.04.037.

## References

[1] D.P. McGregor, Discovering and improving novel peptide therapeutics, Curr. Opin. Pharmacol. 8 (2008) 616–619.
[2] M. Langer, A.G. Beck-Sickinger, Peptides as carrier for tumor diagnosis and treatment, Curr. Med. Chem. Anticancer Agents 1 (2001) 71–93.
[3] V.M. Ahrens, K. Bellmann-Sickert, A.G. Beck-Sickinger, Peptides and peptide conjugates: therapeutics on the upward path, Future Med. Chem. 4 (2012) 1567–1586.
[4] S.E. Ong, The expanding field of SILAC, Anal. Bioanal. Chem. 404 (2012) 967–976.
[5] S.E. Ong, B. Blagoev, I. Kratchmarova, D.B. Kristensen, H. Steen, A. Pandey, M. Mann, Stable isotope labeling by amino acids in cell culture, SILAC, as a simple and accurate approach to expression proteomics, Mol. Cell. Proteomics 1 (2002) 376–386.
[6] S.E. Ong, M. Mann, A practical recipe for stable isotope labeling by amino acids in cell culture (SILAC), Nat. Protoc. 1 (2006) 2650–2660.
[7] IARC, World cancer report, International Agency for Research on Cancer, Lyon, 2008.
[8] J.C. Reubi, M. Gugger, B. Waser, J.C. Schaer, Y(1)-mediated effect of neuropeptide Y in cancer: breast carcinomas as targets, Cancer Res. 61 (2001) 4636–4641.
[9] V.M. Ahrens, R. Frank, S. Boehnke, C.L. Schutz, G. Hampel, D.S. Iffland, N.H. Bings, E. Hey-Hawkins, A.G. Beck-Sickinger, Receptor-mediated uptake of boron-rich neuropeptide y analogues for boron neutron capture therapy, ChemMedChem 10 (2015) 164–172.
[10] X. Pedragosa-Badia, J. Stichel, A.G. Beck-Sickinger, Neuropeptide Y receptors: how to get subtype selectivity, Front. Endocrinol. (Lausanne) 4 (2013) 5.
[11] R.M. Söll, M.C. Dinger, I. Lundell, D. Larhammer, A.G. Beck-Sickinger, Novel analogues of neuropeptide Y with a preference for the Y1-receptor, Eur. J. Biochem. 268 (2001) 2828–2837.
[12] I.U. Khan, D. Zwanziger, I. Bohme, M. Javed, H. Naseer, S.W. Hyder, A.G. Beck-Sickinger, Breast-cancer diagnosis by neuropeptide Y analogues: from synthesis to clinical application, Angew. Chem. Int. Ed. Engl. 49 (2010) 1155–1158.
[13] G. Kaur, M. Hollingshead, S. Holbeck, V. Schauer-Vukasinovic, R.F. Camalier, A. Domling, S. Agarwal, Biological evaluation of tubulysin A: a potential anticancer and antiangiogenic natural product, Biochem. J. 396 (2006) 235–242.
[14] D.R. Gehlert, S.L. Gackenheimer, D.A. Schober, [Leu31-Pro34] neuropeptide Y identifies a subtype of 125I-labeled peptide YY binding sites in the rat brain, Neurochem. Int. 21 (1992) 45–67.
[15] S. Hofmann, R. Frank, E. Hey-Hawkins, A.G. Beck-Sickinger, P. Schmidt, Manipulating Y receptor subtype activation of short neuropeptide Y analogs by introducing carbaboranes, Neuropeptides 47 (2013) 59–66.
[16] M.J. Berridge, Rapid accumulation of inositol trisphosphate reveals that agonists hydrolyse polyphosphoinositides instead of phosphatidylinositol, Biochem. J. 212 (1983) 849–858.
[17] M.J. Berridge, R.M. Dawson, C.P. Downes, J.P. Heslop, R.F. Irvine, Changes in the levels of inositol phosphates after agonist-dependent hydrolysis of membrane phosphoinositides, Biochem. J. 212 (1983) 473–482.
[18] I. Böhme, J. Stichel, C. Walther, K. Mörl, A.G. Beck-Sickinger, Agonist induced receptor internalization of neuropeptide Y receptor subtypes depends on third intracellular loop and C-terminus, Cell. Signal. 20 (2008) 1740–1749.

[19] V.M. Ahrens, R. Frank, S. Stadlbauer, A.G. Beck-Sickinger, E. Hey-Hawkins, Incorporation of ortho-carbaboranyl-Nepsilon-modified L-lysine into neuropeptide Y receptor Y1- and Y2-selective analogues, J. Med. Chem. 54 (2011) 2368–2377.
[20] J. He, W.B. Kauffman, T. Fuselier, S.K. Naveen, T.G. Voss, K. Hristova, W.C. Wimley, Direct cytosolic delivery of polar cargo to cells by spontaneous membrane-translocating peptides, J. Biol. Chem. 288 (2013) 29974–29986.
[21] D. Böhme, A.G. Beck-Sickinger, Controlling toxicity of peptide-drug conjugates by different chemical linker structures, ChemMedChem (2015)http://dx.doi.org/10.1002/cmdc.201402514.
[22] L. Ducry, B. Stump, Antibody–drug conjugates: linking cytotoxic payloads to monoclonal antibodies, Bioconjug. Chem. 21 (2010) 5–13.
[23] V. Te Kamp, R. Lindner, H.G. Jahnke, D. Krinke, K.B. Kostelnik, A.G. Beck-Sickinger, A.A. Robitzki, Quantitative impedimetric NPY-receptor activation monitoring and signal pathway profiling in living cells, Biosens. Bioelectron. 67 (2015) 386–393.
[24] S. Majumdar, N. Kobayashi, J.P. Krise, T.J. Siahaan, Mechanism of internalization of an ICAM-1-derived peptide by human leukemic cell line HL-60: influence of physicochemical properties on targeted drug delivery, Mol. Pharm. 4 (2007) 749–758.
[25] I. Böhme, K. Mörl, D. Bamming, C. Meyer, A.G. Beck-Sickinger, Tracking of human Y receptors in living cells—a fluorescence approach, Peptides 28 (2007) 226–234.
[26] F. Sasse, H. Steinmetz, J. Heil, G. Hofle, H. Reichenbach, Tubulysins, new cytostatic peptides from myxobacteria acting on microtubuli. Production, isolation, physicochemical and biological properties, J. Antibiot. 53 (2000) 879–885.
[27] M.W. Khalil, F. Sasse, H. Lunsdorf, Y.A. Elnakady, H. Reichenbach, Mechanism of action of tubulysin, an antimitotic peptide from myxobacteria, Chembiochem 7 (2006) 678–683.
[28] G. Lukinavicius, L. Reymond, E. D'Este, A. Masharina, F. Gottfert, H. Ta, A. Guther, M. Fournier, S. Rizzo, H. Waldmann, C. Blaukopf, C. Sommer, D.W. Gerlich, H.D. Arndt, S.W. Hell, K. Johnsson, Fluorogenic probes for live-cell imaging of the cytoskeleton, Nat. Methods 11 (2014) 731–733.
[29] U. Ziegler, P. Groscurth, Morphological features of cell death, News Physiol. Sci. 19 (2004) 124–128.
[30] D.L. Holliday, V. Speirs, Choosing the right cell line for breast cancer research, Breast Cancer Res. 13 (2011) 215.
[31] H.D. Soule, J. Vazguez, A. Long, S. Albert, M. Brennan, A human cell line from a pleural effusion derived from a breast carcinoma, J. Natl. Cancer Inst. 51 (1973) 1409–1416.
[32] A.K. Croker, D. Goodale, J. Chu, C. Postenka, B.D. Hedley, D.A. Hess, A.L. Allan, High aldehyde dehydrogenase and expression of cancer stem cell markers selects for breast cancer cells with enhanced malignant and metastatic ability, J. Cell. Mol. Med. 13 (2009) 2236–2252.
[33] P. Prabhakaran, F. Hassiotou, P. Blancafort, L. Filgueira, Cisplatin induces differentiation of breast cancer cells, Front. Oncol. 3 (2013) 134.
[34] H. Amlal, S. Faroqui, A. Balasubramaniam, S. Sheriff, Estrogen up-regulates neuropeptide Y Y1 receptor expression in a human breast cancer cell line, Cancer Res. 66 (2006) 3706–3714.
[35] C. Gajate, F. An, F. Mollinedo, Differential cytostatic and apoptotic effects of ecteinascidin-743 in cancer cells. Transcription-dependent cell cycle arrest and transcription-independent JNK and mitochondrial mediated apoptosis, J. Biol. Chem. 277 (2002) 41580–41589.
[36] Y. Fernandez, B. Gu, A. Martinez, A. Torregrosa, A. Sierra, Inhibition of apoptosis in human breast cancer cells: role in tumor progression to the metastatic state, Int. J. Cancer 101 (2002) 317–326.
[37] A.L. Blajeski, V.A. Phan, T.J. Kottke, S.H. Kaufmann, G(1) and G(2) cell-cycle arrest following microtubule depolymerization in human breast cancer cells, J. Clin. Invest. 110 (2002) 91–99.
[38] R.U. Janicke, MCF-7 breast carcinoma cells do not express caspase-3, Breast Cancer Res. Treat. 117 (2009) 219–221.
[39] J.G. Walsh, S.P. Cullen, C. Sheridan, A.U. Luthi, C. Gerner, S.J. Martin, Executioner caspase-3 and caspase-7 are functionally distinct proteases, Proc. Natl. Acad. Sci. U. S. A. 105 (2008) 12815–12819.
[40] S.P. Cullen, S.J. Martin, Caspase activation pathways: some recent progress, Cell Death Differ. 16 (2009) 935–938.
[41] S. Sun, N.P. Lee, R.T. Poon, S.T. Fan, Q.Y. He, G.K. Lau, J.M. Luk, Oncoproteomics of hepatocellular carcinoma: from cancer markers' discovery to functional pathways, Liver Int. 27 (2007) 1021–1038.
[42] E. Hill, M. Clarke, F.A. Barr, The Rab6-binding kinesin, Rab6-KIFL, is required for cytokinesis, EMBO J. 19 (2000) 5711–5719.
[43] N. Kim, K. Song, KIFC1 is essential for bipolar spindle formation and genomic stability in the primary human fibroblast IMR-90 cell, Cell Struct. Funct. 38 (2013) 21–30.
[44] C.I. Wang, K.Y. Chien, C.L. Wang, H.P. Liu, C.C. Cheng, Y.S. Chang, J.S. Yu, C.J. Yu, Quantitative proteomics reveals regulation of karyopherin subunit alpha-2 (KPNA2) and its potential novel cargo proteins in nonsmall cell lung cancer, Mol. Cell. Proteomics 11 (2012) 1105–1122.
[45] L. Zannini, D. Lecis, S. Lisanti, R. Benetti, G. Buscemi, C. Schneider, D. Delia, Karyopherin-alpha2 protein interacts with Chk2 and contributes to its nuclear import, J. Biol. Chem. 278 (2003) 42346–42351.
[46] J.A. Opsahl, S. Ljostveit, T. Solstad, K. Risa, P. Roepstorff, K.E. Fladmark, Identification of dynamic changes in proteins associated with the cellular cytoskeleton after exposure to okadaic acid, Mar. Drugs 11 (2013) 1763–1782.
[47] R.C. Taylor, S.P. Cullen, S.J. Martin, Apoptosis: controlled demolition at the cellular level, Nat. Rev. Mol. Cell Biol. 9 (2008) 231–241.
[48] A. Nagy, A. Plonowski, A.V. Schally, Stability of cytotoxic luteinizing hormone-releasing hormone conjugate (AN-152) containing doxorubicin 14-O-hemiglutarate in mouse and human serum in vitro: implications for the design of preclinical studies, Proc. Natl. Acad. Sci. U. S. A. 97 (2000) 829–834.
[49] A.V. Schally, J.B. Engel, G. Emons, N.L. Block, J. Pinski, Use of analogs of peptide hormones conjugated to cytotoxic radicals for chemotherapy targeted to receptors on tumors, Curr. Drug Deliv. 8 (2011) 11–25.
[50] G. Emons, G. Gorchev, P. Harter, P. Wimberger, A. Stahle, L. Hanker, F. Hilpert, M.W. Beckmann, P. Dall, C. Grundker, H. Sindermann, J. Sehouli, Efficacy and safety of AEZS-108 (LHRH agonist linked to doxorubicin) in women with advanced or recurrent endometrial cancer expressing LHRH receptors: a multicenter phase 2 trial (AGO-GYN5), Int. J. Gynecol. Cancer 24 (2014) 260–265.
[51] V. Mäde, S. Babilon, N. Jolly, L. Wanka, K. Bellmann-Sickert, L.E. Diaz Gimenez, K. Morl, H.M. Cox, V.V. Gurevich, A.G. Beck-Sickinger, Peptide modifications differentially alter G protein-coupled receptor internalization and signaling bias, Angew. Chem. Int. Ed. Engl. 53 (2014) 10067–10071.